Coupled axial-bending dynamic stiffness matrix and its applications for a Timoshenko beam with mass and elastic axes eccentricity

J.R. Banerjee [a,*], A. Ananthapuvirajah [a], X. Liu [b], C. Sun [b]

[a] *Department of Mechanical Engineering and Aeronautics, School of Mathematics, Computer Science and Engineering, City, University of London, Northampton Square, London, EC1V 0HB, UK*
[b] *School of Traffic and Transport Engineering, Central South University, Changsha, Hunan, 410075, China*

A B S T R A C T

The dynamic stiffness matrix of a coupled axial-bending Timoshenko beam is developed to investigate the free vibration behaviour of such beams and their assemblies. Applying Hamilton's principle, the governing differential equations of motion of a Timoshenko beam in free vibration is derived by considering the axial-bending coupling effect arising from the mass axis eccentricity with the elastic axis of the beam cross-section. The differential equations are then solved in an exact sense, giving expressions for the axial and bending displacements as well as the bending rotation. The expressions for axial force, shear force and bending moment are formed using the natural boundary conditions which resulted from the Hamiltonian formulation. Next, the frequency-dependent dynamic stiffness matrix of the coupled axial-bending Timoshenko beam is derived by relating the amplitudes of the axial force, shear force and bending moment to the corresponding amplitudes of axial displacement, bending displacement and bending rotation. The resulting dynamic stiffness matrix is effectively applied to investigate the free vibration behaviour of axial-bending coupled Timoshenko beams by making use of the Wittrick-Williams algorithm as solution technique. The results with emphasis on the axial-bending coupling effects and the importance of the shear deformation and rotatory inertia in free vibration behaviour of coupled axial-bending Timoshenko beams and frameworks are discussed with significant conclusions drawn.

1. Introduction

There are many engineering structures that can be modelled as beams for the analysis of their dynamic behaviour by using classical Bernoulli-Euler or Timoshenko theories, but some of these structures which have mass axis eccentricity relative to the elastic axis cannot be modelled satisfactorily by these conventional theories because the coupling effect arising from different modes of deformations due to the non-coincident mass and elastic axes is ignored in these theories. In this respect, considerable amount of research has been carried out for dynamic analysis of coupled bending-torsion beams for well over three decades [1–4]. The underlying motivation which stimulated these initiatives is by and large due to their aeronautical applications where a high aspect aircraft wing such as that of a transport airliner or a sailplane can be modelled quite accurately as an assembly of bending-torsion coupled beams to carry out their free vibration [5], aeroelastic [6] and optimisation studies [7]. By contrast, the axial-bending coupling arising from the non-coincident mass and elastic axes has not been

apparently given enough attention and thus, has not featured widely in the literature. The purpose of this paper is to redress this imbalance. One of the reasons why the bending-torsion coupling dominates the literature as opposed to axial-bending coupling is that unlike bending-torsion coupling, the coupling between the axial and bending deformation does not generally occur in aircraft wings and therefore, such coupling is considered inconsequential when investigating their dynamic characteristics.

With the above pretext, it should be recognised that there is a variety of wide-ranging structures used in civil, offshore and marine engineering applications, amongst others for which the axial-bending coupling contrary to bending-torsion coupling is of greater significance. As mentioned above, the literature in this area is unfortunately lacking, and a survey shows that only a handful of papers have been published [8–15] which deal with the free vibration problem of axial-bending coupled beams. These are briefly reviewed next.

By means of the assumed modes method, Yigit and Christoforou [8] investigated the transverse vibration of an oil-well drill string by

---

modelling it as a slender axial-bending coupled beam with the inclusion of non-linear coupling terms and considering the lower portion of the beam simply-supported in the analysis. Han and Benaroya [9] studied the coupled transverse-axial vibration of a compliant tower which they also modelled as a beam, but with a concentrated mass at the free end, and with the other end hinged. Although they formulated the problem by using nonlinear coupled theory, they eventually concluded that the linear theory was adequate even when the axial motion was no longer negligible. Trindade et al. [10] published their research on the non-linear vibration of a drill-string idealised by a vertical slender cylinder which was clamped at its upper extreme but pinned at its lower extreme. They applied constrain inside the outer cylinder in its lower portion and used Karhunen-Loeve decomposition to simulate the dynamics of the system. Notably, they emphasized the importance of including the axial-bending coupling terms when investigating the vibration characteristics of drill-strings. Later, Sampaio et al. [11] used a geometrically non-linear model to study the axial-torsional coupled vibration of drill-strings. Ginsberg [12] used a different approach when he investigated the axial-transverse vibration of a beam by introducing different amounts of coupling between the axial and transverse displacements through suitable choice of the boundary conditions. He manipulated the boundary conditions by using a simple support at one end of the beam and a tilted roller support at the other when computing the natural frequencies, mode shapes and the forced response of the beam. Lenci and Rega [13] on the other hand used an asymptotic method to study the axial-transverse coupled vibration of Timoshenko beams with arbitrary slenderness ratios and boundary conditions. They illustrated both the nonlinear and linear behaviour of axial-transverse coupled Timoshenko beams. Lei et al. [14] investigated the free and forced vibration behaviour of a two-layered axial-bending coupled Timoshenko beam for which the mass and stiffness distributions through the thickness of the beam cross-section were non-uniform. Subsequently, Ni and Hua [15] advanced the work of Lei et al. [14] by including multi-layered beams with arbitrary boundary conditions in their theory when investigating the coupled axial-bending vibration. (Note that research in the area of axial-bending coupled beams in the context of multi-body dynamics is outside the scope of the current paper, but interested readers are referred to a recent paper [16] which gives necessary information and cross references on the subject.) Recently the first two authors of this paper contributed to the existing literature by developing the dynamic stiffness method (DSM) of a coupled axial-bending beam [17] in order to investigate its free vibration characteristics. Their dynamic stiffness theory included the axial-bending coupling effects arising from the non-coincident mass and elastic axes of the beam cross-section, and they found significant differences in the results when compared with the corresponding results obtained from the classical Bernoulli-Euler theory. Their investigation appears to be the first of its kind in the development of the dynamic stiffness method for coupled axial-bending vibration of beams. However, their work significant though it was, had a deficiency in that it excluded the effects of shear deformation and rotatory inertia which can be significant for short and stubby beams. Nevertheless, their work was a significant step forward to develop the dynamic stiffness theory for a coupled axial-bending Timoshenko beam which includes the effects of shear deformation and rotatory inertia. This is essentially the central theme of this paper. This new development is quite difficult because the level of complexity of the problem increases considerably and it necessitated considerable time and efforts. The authors have undertaken this research to first develop and then apply the DSM to study the free vibration characteristics of coupled axial-bending Timoshenko beams and their assemblies in order to demonstrate the effects of shear deformation and rotatory inertia on results. The DSM is well known for its accuracy and computational efficiency [1,2,17–19]. A subsidiary, but important contribution made in this paper is to show that the entire analysis can be carried out in the real domain by using explicit algebraic stiffness expressions instead of using the complex domain analysis reported in the literature [14,15] which
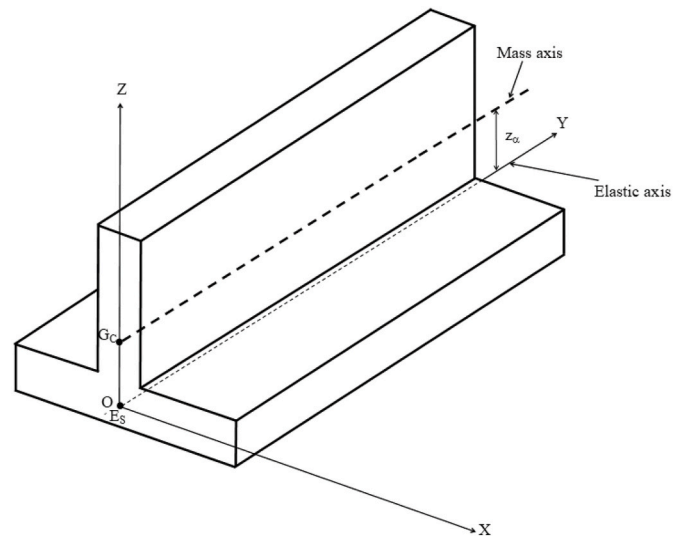

Fig. 1. Coordinate system and notation for a coupled axial-bending Timoshenko beam.

relied rather needlessly on unwarranted complex matrix operations. Furthermore, some unintentional misconceptions reported in the literature regarding the number of constants needed for the solution to describe the axial and bending deformations of a coupled axial-bending beam are addressed in this paper. The authors have managed to provide an alternative, but improved solution for the problem. The paper is organised as follows. First, the theory begins with the derivation of the governing differential equations of motion of a coupled axial-bending Timoshenko beam in free vibration by applying Hamilton's principle. For harmonic oscillation, the equations are solved in explicit analytical form, providing expressions for the amplitudes of axial displacement, bending displacement, bending rotation as well as axial force, shear force and bending moment. The frequency dependent dynamic stiffness is then formulated by relating the amplitudes of the forces to those of the displacements at the ends of the axial-bending coupled Timoshenko beam. The resulting dynamic stiffness matrix is operated by the Wittrick-Williams algorithm [20] as solution technique when computing the natural frequencies and mode shapes of some illustrative examples. Finally, some conclusions are drawn.

2. Theory

In what follows, the dynamic stiffness matrix of a freely vibrating Timoshenko beam when its free vibratory motion is coupled between axial and bending deformations is derived using linear small deflection theory.

2.1. Derivation of the governing differential equations of motion and natural boundary conditions for a coupled axial-bending Timoshenko beam

Fig. 1 shows a uniform coupled axial-bending Timoshenko beam of length L in a right-handed Cartesian coordinate system with the Y-axis coinciding with the beam elastic axis. The coupling between axial and bending displacements in such a beam will occur because of the eccentricity of the centroid (G_c) and shear centre (E_s) of the beam cross-section, as shown. There are many practical cross-sections for which the centroid and shear centre are non-coincident (see Fig. 2 of [17]), but the inverted T section is shown in Fig. 1 only for convenience. The mass axis and the elastic axis of the beam which are respectively the loci of the centroid and shear centre of the beam cross-section are separated by a

distance z_α as shown.

If v, w and θ are axial displacement, bending displacement and bending rotation of a point at a distance y from the origin and at a height z from the elastic axis, i.e. the point (y, z) in the coordinate system (Fig. 1), one can write

$$v = v_0 - z\theta, \quad w = w_0 \tag{1}$$

where v_0 and w_0 are the corresponding displacement components of the point $(y, 0)$ on the Y-axis (i.e. on the elastic axis).

Using linear, small deflection elasticity theory, the expression for the normal strain ε_y and shearing strain (γ_{yz}) can be expressed as

$$\varepsilon_y = v_0' - z\theta', \quad \gamma_{yz} = w_0' - \theta \tag{2}$$

where a prime denotes differentiation with respect to y.

The potential or strain energy of the beam due to normal and shear strains is given by

$$U = \frac{1}{2}\int_0^L \int_A E\varepsilon_y^2 \, dA \, dy + \frac{1}{2}\int_0^L \int_A kG\gamma_{yz}^2 \, dA \, dy \tag{3}$$

where E and G are the Young's modulus and shear modulus of the beam material, respectively and k is shear correction or shape factor, and the integrations are carried out over the beam cross-sectional area A and length L.

Substituting ε_y and γ_{yz} from Eq. (2) into Eq. (3), and integrating over the beam cross-section, we obtain

$$U = \frac{1}{2}\int_0^L \left\{ EA\left(v_0'\right)^2 - 2EAz_\alpha v_0'\theta' + EI_e\left(\theta'\right)^2 + kAG\left(w_0' - \theta\right)^2 \right\} dy \tag{4}$$

where A and I_e are the area of cross-section and second moment of area about the elastic axis so that EA and EI_e are the extensional and bending stiffnesses of the beam, respectively.

The kinetic energy of the beam is given by

$$T = \frac{1}{2}\int_0^L \int_A \rho\left\{ (\dot{v})^2 + (\dot{w})^2 \right\} dy \tag{5}$$

where ρ is the density of the beam material and an over dot represents differentiation with respect to time t.

Equation (5) with the help of Eq. (1) becomes

$$T = \frac{1}{2}\int_0^L \left\{ \rho A\left(\dot{v}_0\right)^2 - 2\rho Az_\alpha \dot{v}_0\dot{\theta} + \rho I_e\left(\dot{\theta}\right)^2 + \rho A\left(\dot{w}_0\right)^2 \right\} dy \tag{6}$$

Hamilton's principle states

$$\delta \int_{t_1}^{t_2} (T - U) \, dt = 0 \tag{7}$$

where t_1 and t_2 are the time interval in the dynamic trajectory, and δ is the usual variational operator.

The governing differential equations of motion for the coupled axial-bending Timoshenko beam and the associated boundary condition in free vibration can now be derived by substituting the potential (U) and kinetic (T) energy expressions of Eqs. (4) and (6) into Eq. (7), using the δ operator, integrating by parts and then collecting terms. In an earlier publication, the entire procedure to generate the governing differential equations of motion and natural boundary conditions for bar or beam type structures was automated by Banerjee et al. [21] by applying symbolic computation. In this way, the governing differential equations of motion of the axial-bending coupled beam and the associated natural boundary conditions are obtained as follows.

Governing differential equations:

$$EAv_0'' - EAz_\alpha\theta'' - \rho A\ddot{v}_0 + \rho Az_\alpha\ddot{\theta} = 0 \tag{8}$$

$$EI_e\theta'' - \rho I_e\ddot{\theta} + \rho Az_\alpha\ddot{v}_0 - EAz_\alpha v_0'' + kAG\left(w_0' - \theta\right) = 0 \tag{9}$$

$$kAG\left(w_0'' - \theta'\right) - \rho A\ddot{w}_0 = 0 \tag{10}$$

Natural boundary conditions:

Axial force: $F = -EAv_0' + EAz_\alpha\theta'$ (11)

Bending moment: $M = -EI_e\theta' + EAz_\alpha v_0'$ (12)

Shear force: $S = -kAG\left(w_0' - \theta\right)$ (13)

Assuming harmonic oscillation with circular or angular frequency ω rad/s, one can write

$$v_0 = Ve^{i\omega t}; \quad w_0 = We^{i\omega t}; \quad \theta = \Theta e^{i\omega t} \tag{14}$$

where V, W and Θ are the amplitudes of the axial displacement, bending displacement and bending rotation, respectively.

Substituting Eq. (14) into Eqs. (8)–(10) and introducing the non-dimensional length $\xi = y/L$ and the differential operator $D = \frac{d}{d\xi}$, yield the following ordinary differential equations in V, W and Θ

$$\left(\omega^2\rho A + \frac{EA}{L^2}D^2\right)V - \left(\omega^2\rho Az_\alpha + \frac{EAz_\alpha}{L^2}D^2\right)\Theta = 0 \tag{15}$$

$$-\left(\omega^2\rho Az_\alpha + \frac{EAz_\alpha}{L^2}D^2\right)V + \left(\frac{kAG}{L}D\right)W + \left(\frac{EI_e}{L^2}D^2 + \omega^2\rho I_e - kAG\right)\Theta = 0 \tag{16}$$

$$\left(\frac{kAG}{L^2}D^2 + \omega^2\rho A\right)W - \left(\frac{kAG}{L}D\right)\Theta = 0 \tag{17}$$

We introduce the following non-dimensional parameter to recast Eqs. (15)–(17) in a different, but more favourable form

$$\left. \begin{aligned} &a^2 = \frac{\omega^2\rho AL^2}{EA}, \ b^2 = \frac{\omega^2\rho AL^4}{EI_e}, \\ &r^2 = \frac{EI_e}{EAL^2} = \frac{I_e}{AL^2} = \frac{a^2}{b^2}, \\ &s^2 = \frac{EI_e}{kAGL^2}, \ \mu^2 = \frac{z_\alpha^2}{L^2} \end{aligned} \right\} \tag{18}$$

Substituting Eq. (18) into Eqs. (15)–(17) gives

$$\left(D^2 + a^2\right)V = z_\alpha\left(D^2 + a^2\right)\Theta \tag{19}$$

$$\frac{Lr^2}{s^2}DW + L^2\left(r^2D^2 + a^2r^2 - \frac{r^2}{s^2}\right)\Theta = z_\alpha\left(D^2 + a^2\right)V \tag{20}$$

$$\left(D^2 + b^2s^2\right)W = LD\Theta \tag{21}$$

By eliminating V from Eq. (20) with the help of Eq. (19) and then after some mathematical manipulation, a fourth order ordinary differential equation can be obtained from Eqs. (20) and (21) as follows, which is identically satisfied by both W and Θ.

$$\left[D^4 + \left(a^2 + b^2s^2\right)D^2 - b^2\left(\frac{r^2}{r^2 - \mu^2} - a^2s^2\right)\right]H = 0 \tag{22}$$

where

$$H = W \ or \ \Theta \tag{23}$$

The differential equation, Eq. (22) can be solved for H and hence for W and Θ, using standard procedure to give
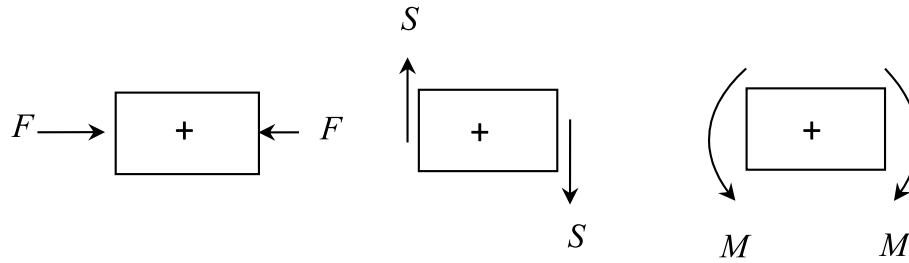
Fig. 2. Sign convention for positive axial force *F*, shear force *S* and bending moment *M*.

$$W(\xi) = A_1 \cosh \alpha\xi + A_2 \sinh \alpha\xi + A_3 \cos \beta\xi + A_4 \sin \beta\xi \tag{24}$$

$$\Theta(\xi) = B_1 \sinh \alpha\xi + B_2 \cosh \alpha\xi + B_3 \sin \beta\xi + B_4 \cos \beta\xi \tag{25}$$

where $A_1 - A_4$ and $B_1 - B_4$ are two different sets of constants and α and β are given by

$$\alpha^2 = -\frac{\left(a^2 + b^2 s^2\right)}{2} + \frac{\sqrt{\left(a^2 + b^2 s^2\right)^2 + 4b^2\left(\frac{r^2}{r^2 - \mu^2} - a^2 s^2\right)}}{2} \tag{26}$$

$$\beta^2 = \frac{\left(a^2 + b^2 s^2\right)}{2} + \frac{\sqrt{\left(a^2 + b^2 s^2\right)^2 + 4b^2\left(\frac{r^2}{r^2 - \mu^2} - a^2 s^2\right)}}{2} \tag{27}$$

It can be shown with the help of Eq. (21) that the constants $A_1 - A_4$ and $B_1 - B_4$ appearing in Eqs. (24) and (25) are related as follows.

$$B_1 = (k_\alpha / L)A_1, \quad B_2 = (k_\alpha / L)A_2, \quad B_3 = (k_\beta / L)A_3, \quad B_4 = -(k_\beta / L)A_4 \tag{28}$$

where k_α and k_β are given by

$$k_\alpha = \frac{b^2 s^2 + \alpha^2}{\alpha}, \quad k_\beta = \frac{b^2 s^2 - \beta^2}{\beta} \tag{29}$$

The solution for the axial displacement *V* can be obtained from Eq. (19) by introducing a new variable *U* where

$$U = V - z_\alpha \Theta \tag{30}$$

Substituting Eq. (30) into (19) gives

$$\left(D^2 + a^2\right) U = 0 \tag{31}$$

The solution of Eq. (31) is given by

$$U(\xi) = A_5 \cos \gamma\xi + A_6 \sin \gamma\xi \tag{32}$$

where

$$\gamma = a \tag{33}$$

Now, by making use of Eq. (30), the solution for *V* can be obtained from the solution of *U* in Eq. (32) which with the help of Eqs. (25) and (28) give

$$V(\xi) = \mu k_\alpha A_1 \sinh \alpha\xi + \mu k_\alpha A_2 \cosh \alpha\xi + \mu k_\beta A_3 \sin \beta\xi - \mu k_\beta A_4 \cos \beta\xi + A_5 \sin \gamma\xi + A_6 \cos \gamma\xi \tag{34}$$

At this stage, an important comment is in order. Clearly, the solutions for the bending displacement (*W*) and bending rotation (Θ) consist of four constants each (see Eqs. (24) and (25)) whereas the solution for the axial displacement *V* in Eq. (34) requires six constants. This is a noteworthy and important finding because in all previous investigations [14, 15] of free vibration analysis for axial-bending coupled beams, it was decided that six constants are needed to describe each of the three displacement components *V*, *W* and Θ. As it turned out, this was an inadvertent oversight by earlier investigators. Admittedly, the first two authors of this paper were also in this category [17] until this recent work. Understandably, research is constantly evolving, and progress made often replaces or improves earlier findings by later findings. It is also worth noting that in earlier works [14,15], the solutions of the governing differential equations (Eqs. (15)–(17)) were sought in the complex domain unlike the much-simplified real domain solutions given here, see Eqs. (24), (25) and (34).

The amplitudes of the axial force (*F*), shear force (*S*) and bending moment (*M*) are obtained as follows by using Eqs. (11)–(13) and the
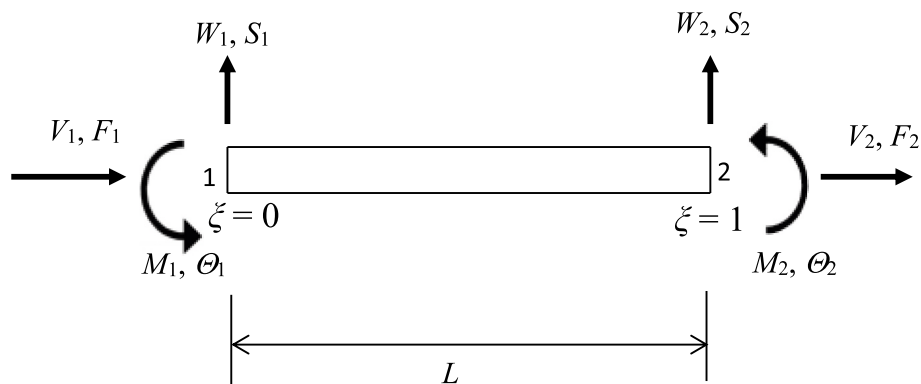

Fig. 3. Boundary condition for displacements and forces for a coupled axial-bending Timoshenko beam.

explicit solutions for V, W and Θ given above.

$$F(\xi) = -\frac{EA}{L}\left(\frac{dV}{d\xi} - \mu\frac{d\Theta}{d\xi}\right) = -\frac{EA}{L}\gamma(A_5\cos\gamma\xi - A_6\sin\gamma\xi) \tag{35}$$

$$S(\xi) = -kAG\left(\frac{1}{L}\frac{dW}{d\xi} - \Theta\right) = \frac{EI_e}{L^3}\frac{1}{s^2}\left(\Theta L - \frac{dW}{d\xi}\right)$$
$$= \frac{EI_e}{L^3}(A_1 g_\alpha\sinh\alpha\xi + A_2 g_\alpha\cosh\alpha\xi + A_3 g_\beta\sin\beta\xi - A_4 g_\beta\cos\beta\xi) \tag{36}$$

$$M(\xi) = -\frac{EI}{L^2}\left(L\frac{d\Theta}{d\xi} - \frac{\mu}{r^2}\frac{dV}{d\xi}\right)$$
$$= -\frac{EI}{L^2}(A_1 h_\alpha\cosh\alpha\xi + A_2 h_\alpha\sinh\alpha\xi + A_3 h_\beta\cos\beta\xi + A_4 h_\beta\sin\beta\xi - A_5 h_\gamma\cos\gamma\xi + A_6 h_\gamma\sin\gamma\xi) \tag{37}$$

where

$$g_\alpha = \frac{k_\alpha - \alpha}{s^2}, \; g_\beta = \frac{k_\beta + \beta}{s^2} \tag{38}$$

$$h_\alpha = \alpha k_\alpha\left(1 - \frac{\mu^2}{r^2}\right), \quad h_\beta = \beta k_\beta\left(1 - \frac{\mu^2}{r^2}\right), \quad h_\gamma = \frac{\gamma\mu}{r^2} \tag{39}$$

2.2. Derivation of the dynamic stiffness matrix

The expressions for the axial displacement (V), bending displacement (W) and bending rotation (Θ) together with the expressions for axial force (F), shear force (S) and bending moment (M) given above can now be used to derive the dynamic stiffness matrix of the coupled axial-bending Timoshenko beam by applying the boundary conditions at the two ends of the elastic axis of the beam. Referring to the sign convention for positive axial force, shear force and bending moment shown in Fig. 2, the following boundary conditions for displacements and forces as shown in Fig. 3 are applied:

At $\xi = 0$:
$V = V_1$; $W = W_1$; $\Theta = \Theta_1$; $F = F_1$; $S = S_1$; $M = M_1$ $\tag{40}$

At $\xi = 1$:
$V = V_2$; $W = W_2$; $\Theta = \Theta_2$; $F = -F_2$; $S = -S_2$; $M = -M_2$ $\tag{41}$

The displacement vector $\boldsymbol{\delta}$ and the force vector $\mathbf{P}$ of the beam connecting the ends 1 and 2, see Fig. 3, can be expressed as:

$$\boldsymbol{\delta} = [V_1 \; W_1 \; \Theta_1 \; V_2 \; W_2 \; \Theta_2]^T \quad \mathbf{P} = [F_1 \; S_1 \; M_1 \; F_2 \; S_2 \; M_2]^T \tag{42}$$

where the upper suffix T denotes a transpose.

The displacement vector $\boldsymbol{\delta}$ and the constant vector $\mathbf{A}$ (with A_i, $i = 1,2,$ ...6) can now be related using Eqs. (24), (25), (34) and Eqs. (40), (41) to give

$$\boldsymbol{\delta} = \mathbf{Q}\,\mathbf{A} \tag{43}$$

where

$$\mathbf{Q} = \begin{bmatrix} 0 & \mu k_\alpha & 0 & -\mu k_\beta & 0 & 1 \\ 1 & 0 & 1 & 0 & 0 & 0 \\ 0 & k_\alpha/L & 0 & -k_\beta/L & 0 & 0 \\ \mu k_\alpha S_{h\alpha} & \mu k_\alpha C_{h\alpha} & \mu k_\beta S_\beta & -\mu k_\beta C_\beta & S_\gamma & C_\gamma \\ C_{h\alpha} & S_{h\alpha} & C_\beta & S_\beta & 0 & 0 \\ k_\alpha S_{h\alpha}/L & k_\alpha C_{h\alpha}/L & k_\beta S_\beta/L & -k_\beta C_\beta/L & 0 & 0 \end{bmatrix} \tag{44}$$

with

$$S_{h\alpha} = \sinh\alpha, \; C_{h\alpha} = \cosh\alpha, \; S_\beta = \sin\beta,$$
$$C_\beta = \cos\beta, \; S_\gamma = \sin\gamma, \; C_\gamma = \cos\gamma \tag{45}$$

In a similar manner, the relationship between the force vector $\mathbf{P}$ and the constant vector $\mathbf{A}$ is established by using Eqs. (35)–(37) and Eqs. (40), (41) to give

$$\mathbf{P} = \mathbf{R}\,\mathbf{A} \tag{46}$$

where

$$\mathbf{R} = \begin{bmatrix} 0 & 0 & 0 & 0 & -\frac{EA}{L}\gamma & 0 \\ 0 & \frac{EI_e}{L^3}g_\alpha & 0 & -\frac{EI_e}{L^3}g_\beta & 0 & 0 \\ -\frac{EI_e}{L^2}h_\alpha & 0 & -\frac{EI_e}{L^2}h_\beta & 0 & \frac{EI_e}{L^2}h_\gamma & 0 \\ 0 & 0 & 0 & 0 & \frac{EA}{L}\gamma C_\gamma & -\frac{EA}{L}\gamma S_\gamma \\ -\frac{EI_e}{L^3}g_\alpha S_{h\alpha} & -\frac{EI_e}{L^3}g_\alpha C_{h\alpha} & -\frac{EI_e}{L^3}g_\beta S_\beta & \frac{EI_e}{L^3}g_\beta C_\beta & 0 & 0 \\ \frac{EI_e}{L^2}h_\alpha C_{h\alpha} & \frac{EI_e}{L^2}h_\alpha S_{h\alpha} & \frac{EI_e}{L^2}h_\beta C_\beta & \frac{EI_e}{L^2}h_\beta S_\beta & -\frac{EI_e}{L^2}h_\gamma C_\gamma & \frac{EI_e}{L^2}h_\gamma S_\gamma \end{bmatrix} \tag{47}$$

By eliminating the constant vector, $\mathbf{A}$ from Eqs. (43) and (46), $\mathbf{P}$ and $\boldsymbol{\delta}$ can now be related to give the dynamic stiffness matrix relationship of the axial-bending coupled Timoshenko beam as

$$\mathbf{P} = \mathbf{K}\,\boldsymbol{\delta} \tag{48}$$

where

$$\mathbf{K} = \mathbf{R}\,\mathbf{Q}^{-1} \tag{49}$$

is the resulting frequency-dependent dynamic stiffness matrix. It is to be noted that the dynamic stiffness matrix $\mathbf{K}$ of Eq. (49) will be always symmetric. The dynamic stiffness matrix in expanded form, giving the relationship between the amplitudes of the forces to those of the displacements at the two nodes of the beam can now be expressed as.

$$\begin{bmatrix} F_1 \\ S_1 \\ M_1 \\ F_2 \\ S_2 \\ M_2 \end{bmatrix} = \begin{bmatrix} k_{11} & k_{12} & k_{13} & k_{14} & k_{15} & k_{16} \\ k_{12} & k_{22} & k_{23} & k_{24} & k_{25} & k_{26} \\ k_{13} & k_{23} & k_{33} & k_{34} & k_{35} & k_{36} \\ k_{14} & k_{24} & k_{34} & k_{44} & k_{45} & k_{46} \\ k_{15} & k_{25} & k_{35} & k_{45} & k_{55} & k_{56} \\ k_{16} & k_{26} & k_{36} & k_{46} & k_{56} & k_{66} \end{bmatrix} \begin{bmatrix} V_1 \\ W_1 \\ \Theta_1 \\ V_2 \\ W_2 \\ \Theta_2 \end{bmatrix} \tag{50}$$

With the advent of the advances in symbolic computation, explicit algebraic expression for each of the independent element of the dynamic stiffness matrix $\mathbf{K}$ was derived by using the symbolic computation package REDUCE [21–23]. Thus, the matrix inversion and matrix multiplication steps of Eq. (49) were carried out with the help of symbolic algebra. The expressions for the stiffness terms which define $\mathbf{K}$ (see Eqs. (49) and (50)) are given by

$$k_{11} = k_{44} = \frac{EA}{L}\gamma \cot \gamma,$$

$$k_{12} = k_{15} = k_{21} = k_{24} = k_{42} = k_{45} = k_{51} = k_{54} = 0,$$

$$k_{13} = k_{31} = k_{46} = k_{64} = -z_\alpha k_{11},$$

$$k_{14} = k_{41} = -\frac{EA}{L}\gamma \operatorname{cosec}\gamma,$$

$$k_{16} = k_{61} = k_{34} = k_{43} = -z_\alpha k_{14},$$

$$k_{22} = k_{55} = \frac{EI_e}{L^3}\frac{\sigma_2\zeta_2}{\Delta},$$

$$k_{23} = k_{32} = -k_{56} = -k_{65} = \frac{EI_e}{L^2}\frac{(\sigma_3\tau_1 + \sigma_4\tau_3)}{\Delta}$$

$$k_{25} = k_{52} = -\frac{EI_e}{L^3}(\sigma_2\zeta_1/\Delta),$$

$$k_{26} = k_{62} = -k_{35} = -k_{53} = \frac{EI_e}{L^2}(\sigma_2\tau_2/\Delta)$$

$$k_{33} = k_{66} = \frac{EI_e}{L}\frac{(\varepsilon_1 + \varepsilon_3 C_\gamma + \varepsilon_4\zeta_3 S_\gamma)}{(S_\gamma\Delta)}$$

$$k_{36} = k_{63} = -\frac{EI_e}{L}\frac{(\varepsilon_2 + \varepsilon_3 + \varepsilon_4\zeta_4)}{(S_\gamma\Delta)}$$

(51)

where

$$\sigma_1 = k_\alpha^2 - k_\beta^2, \ \sigma_2 = k_\alpha g_\beta - k_\beta g_\alpha,$$
$$\sigma_3 = k_\alpha g_\beta + k_\beta g_\alpha, \ \sigma_4 = k_\alpha g_\alpha - k_\beta g_\beta$$

(52)

$$\tau_1 = C_{h\alpha}C_\beta - 1, \ \tau_2 = C_{h\alpha} - C_\beta,$$
$$\tau_3 = S_{h\alpha}S_\beta, \ \tau_4 = S_{h\alpha}S_\beta C_\gamma$$

(53)

$$\varepsilon_1 = \mu\sigma_1\tau_4 h_\gamma, \ \varepsilon_2 = \mu\sigma_1\tau_3 h_\gamma,$$
$$\varepsilon_3 = 2\mu\tau_1 k_\alpha k_\beta h_\gamma, \ \varepsilon_4 = h_\alpha - h_\beta$$

(54)

$$\zeta_1 = k_\alpha S_{h\alpha} - k_\beta S_\beta, \ \zeta_2 = k_\alpha S_{h\alpha}C_\beta - k_\beta C_{h\alpha}S_\beta,$$
$$\zeta_3 = k_\alpha C_{h\alpha}S_\beta + k_\beta S_{h\alpha}C_\beta, \ \zeta_4 = k_\alpha S_\beta S_\gamma + k_\beta S_{h\alpha}S_\gamma$$

(55)

and

$$\Delta = \sigma_1\tau_3 + 2\tau_1 k_\alpha k_\beta$$

(56)

The explicit stiffness expressions given above in Eq. (51) are surprisingly concise and particularly useful when some, but not all the stiffness elements are needed, for example when carrying out sensitivity analysis required for optimisation problems.

The dynamic stiffness matrix **K** developed above, can now be used to compute the natural frequencies and mode shapes of either an individual coupled axial-bending Timoshenko beam, or an assembly of them for different boundary conditions. A long-standing and dependable method to solve the eigenvalue problem accurately and with certainty is to apply the Wittrick-Williams algorithm [20] which has now become an indispensable tool in applying the dynamic stiffness method. The algorithm makes use of the Sturm sequence property of the dynamic stiffness matrix and it ensures that none of the natural frequencies of the structure being analysed is missed. There are numerous papers in the literature with extensive coverage of the algorithm, but for a detailed insight, investigators are referred to the original publication of Wittrick and Williams [20].

3. Results and discussion

The coupled axial-bending dynamic stiffness theory for a Timoshenko beam developed above is now applied to investigate the free vibration behaviour of some illustrative examples. It should be noted that when obtaining results, all support conditions at the ends (nodes) of the beam are applied at the shear centre of the cross-section. This is because the theory developed is based on the deformation of the elastic axis of the beam, which is essentially the locus of the shear centres of the

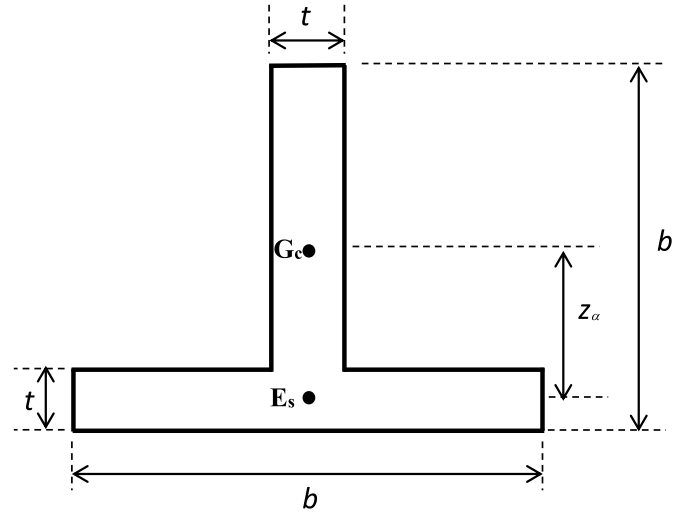**Fig. 4.** Cross-sectional details of a coupled axial-bending Timoshenko beam (mass axis (centroid): G_c, elastic axis (shear centre): E_s).

cross-sections. However, in an investigation of this nature, the validation of the theory with the provision of satisfactory accuracy is essential. Unfortunately, no directly comparable results could be found in the literature. Therefore, in the absence of published results, the authors devised some alternative measures to confirm the validity of their theory in a convincing manner. In order to achieve this, they relied on numerical simulation of results using a well-established space frame computer program called BUNVIS-RG [24,25] which is based on the dynamic stiffness method, but the program is underpinned by classical Bernoulli-Euler and Timoshenko beam theories. Although BUNVIS-RG [24,25] cannot account for the axial-bending coupling effects as in the present case, it has, however, useful capabilities to account for lumped or concentrated mass and/or inertia at a node of a structure and furthermore, it has a feature to connect a Bernoulli-Euler or Timoshenko beam eccentrically between nodes. These two important facilities of BUNVIS-RG [24,25], i.e. the capability to lump a mass and/or inertia at a node and also to connect a member which is offset from the nodes, are exploited here to obtain approximate, but sufficiently accurate comparative results to validate the present theory. The beam cross-section chosen is an inverted T as shown in Fig. 4. The BUNVIS-RG [24,25] model that has been used to validate the theory is illustrated in Fig. 5. In essence, the data file for BUNVIS-RG is appropriately adopted to idealise the elastic and mass axes of the coupled axial-bending Timoshenko beam in a manner that the stiffness distribution of the beam is represented continuously whereas the mass and inertia distribution is represented discretely, as shown in Fig. 5. The coupled axial-bending Timoshenko beam is essentially divided into N uniform elements A_1A_2, A_2A_3, A_3A_4, ...A_NA_{N+1}, which all lie on the elastic axis of the beam. Now, each of the N uniform elements A_1A_2, A_2A_3, A_3A_4, ... A_NA_{N+1} is given the actual stiffness properties (EA, EI and kAG) of the beam, but negligibly small values of the mass and inertia properties (ρA and ρI). For a realistic coupled axial-bending Timoshenko beam and for the type of problems investigated, the negligibly small values for the distributed mass and inertia properties can be typically assigned to be of the order of 10^{-6} or 10^{-7}. Next, the uniform elements A_1A_2, A_2A_3, A_3A_4, ...A_NA_{N+1} are eccentrically connected to nodes 1, 2, 3, ...N+1 of the beam which represent the lumped mass and inertia values of individual elements located at a distance z_α from the elastic axis, as shown in Fig. 5.

Through the above adaptation of BUNVIS-RG [24,25], a coupled axial-bending Timoshenko beam made of aluminium and with the inverted T cross-section of Fig. 4 is now analysed to validate the theory. The dimensions used for the cross-section (see Fig. 4) are $b = 40$ mm, $t = 4$ mm and the length of the beam L is taken as 1 m. The distance between
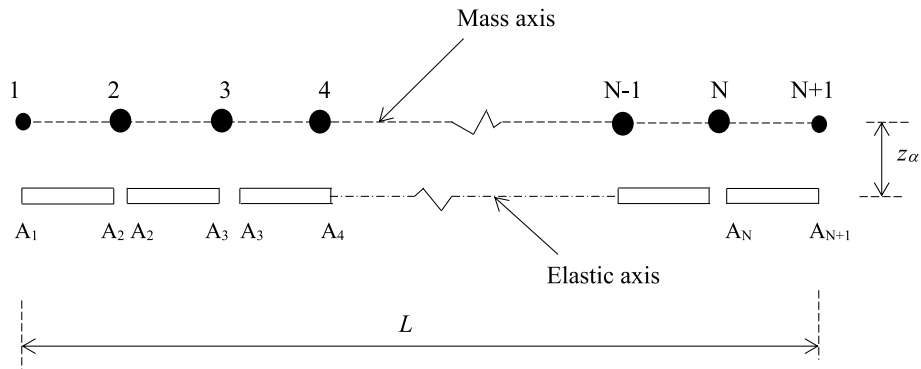
Fig. 5. Idealisation of a coupled axial-bending Timoshenko beam using lumped mass (inertia) and eccentrically connected members for approximate analysis using BUNVIS-RG [24,25].

Table 1
Natural frequencies of a coupled axial-bending Timoshenko beam for Free-Free (F-F), Clamped-Free (C-F), Pinned-Pinned (P-P) and Clamped-Clamped (C-C) boundary conditions.

Boundary condition	Natural frequencies ω_i (rad/s)	Present theory ω_i (rad/s)	Approximate result using BUNVIS-RG [24,25] ω_i (rad/s)	% Difference
F-F	ω_1	1392.3	1383.6	0.62
	ω_2	3784.9	3770.6	0.38
	ω_3	7274.3	7282.6	0.12
	ω_4	11,727	11,859	1.12
	ω_5	15,996	15,937	0.37
C-F	ω_1	220.04	220.04	0.00
	ω_2	1365.0	1370.5	0.41
	ω_3	3761.8	3807.3	1.21
	ω_4	7210.1	7367.8	2.19
	ω_5	7998.1	8023.8	0.32
P-P	ω_1	736.38	739.59	0.43
	ω_2	2431.1	2454.2	0.95
	ω_3	5510.5	5636.6	2.29
	ω_4	9214.8	9508.1	3.18
	ω_5	14,276	15,038	5.34
C-C	ω_1	1381.2	1400.5	1.39
	ω_2	3735.6	3844.7	2.92
	ω_3	7147.6	7489.3	4.78
	ω_4	11,478	12,271	6.91
	ω_5	15,996	15,976	0.12

the shear centre and the centroid of the cross-section is worked out to be $z_\alpha = 9.474$ mm. The material properties used in the analysis are the Young's modulus $E = 70$ GPa, the shear modulus $G = 26.92$ GPa and the density $\rho = 2700$ kg/m^3. The shear correction factor (also known as the shape factor) k is taken to be 2/3. Using the above data, the stiffness and mass properties of the section are calculated as follows:

(i) Axial stiffness $(EA) = 2.128 \times 10^7$ N, (ii) Bending stiffness $(EI_e) = 5135.57$ Nm^2, (iii) Shear stiffness $(kAG) = 5.4564 \times 10^6$ N, (iv) Mass per unit length $(\rho A) = 0.8208$ kg/m and (v) Rotatory inertia per unit length $(\rho I_e) = 0.001981$ kgm.

The first five natural frequencies of the above axial-bending coupled Timoshenko beam with Free-Free (F-F), Clamped-Free (C-F), Pinned-Pinned (P-P) and Clamped-Clamped (C-C) boundary conditions using the present theory are shown in Table 1 alongside the results computed by BUNVIS-RG [24,25]. (Note that the zero frequencies corresponding to the rigid-body modes for the F-F case are discounted (disregarded) in the results shown in Table 1.) The number of elements N used in the BUNVIS-RG model was varied and with increasing values of N, the convergence of results was assured. The results shown in Table 1 were computed using N = 20 which was adequate. The agreement between the results computed from the present theory and the ones using

BUNVIS-RG is excellent for all five natural frequencies and for all boundary conditions, as can be seen in Table 1. Given the complexity of the problem and the difficulty in obtaining comparative results, such surprisingly good agreement is reassuring and no-doubt a useful confirmation of the correctness of the theory. Particular attention should be given to the results for the F-F boundary condition shown in Table 1 because the computation of natural frequencies for this case involved all dynamic stiffness expressions derived in this paper as there were no supports or constraints on the beam for this case. It can now be ascertained from the results reported in Table 1 that the validity of the theory is confirmed both credibly and convincingly.

Now results are computed to demonstrate the effect of the slenderness ratio L/r_0 where L is the length of the beam and r_0 is radius of gyration of the cross-section defined by $r_0 = \sqrt{\frac{I_e}{A}} = \sqrt{\frac{EI_e}{EA}}$ on the natural frequencies of the beam. Note that L/r_0 is the reciprocal of r in Eq. (18). Without changing the cross-section of the beam in the above example, its length (L) is varied from its original value of 1 m in order to alter the values of the slenderness ratio (L/r_0). Using the present theory, Table 2 shows the results for the first five natural frequencies of the beam with slenderness ratios 25, 50, 75 and 100 and for boundary conditions F-F, C-F, P-P and C-C, respectively, alongside the results computed by using the earlier coupled axial-bending Bernoulli-Euler theory [17]. As expected, the differences in results for lower values of the slenderness ratios (and higher natural frequencies) are quite pronounced. For instance, the discrepancies in the fifth natural frequency using the present theory and the earlier theory [17] for F-F, C-F, P-P and C-C boundary conditions for slenderness ratio 25 are 20.9%, 20.8%, 21.4% and 37.4%, respectively. The mode shapes corresponding to the first five natural frequencies for the F-F, C-F, P-P and C-C boundary conditions for this slenderness ratio of 25 computed from the present theory are illustrated in Fig. 6. In the presentation of modes, the bending displacement is shown by solid lines whereas the axial displacement is shown by broken (dashed) lines. As can be seen, substantial coupling between the axial and bending deformation exists in many of the modes shown in Fig. 6. Such coupling cannot be captured by the classical Bernoulli-Euler or Timoshenko theories. Some discussion of mode shapes shown in Fig. 6 would be instructive. For F-F boundary condition, the first and fourth (elastic) modes are respectively bending and axial whereas the second, third and the fifth modes show some amount of coupling between bending and axial deformation. For the C-F case, the first mode shows some coupling between the bending and axial deformations whereas the second mode is predominantly bending. By contrast, the third mode is axial, leaving the fourth and fifth modes bending dominated. The mode shapes for the P-P case reveals a different picture. The first mode is primarily bending with a small amount of axial deformation whereas the second and third show substantial amount of coupling between bending and axial deformation. The fourth mode is axial dominated, but there is considerable amount of bending

Table 2

Effect of the slenderness ratio on the natural frequencies of coupled axial-bending Timoshenko beam for various boundary conditions.

Slenderness Ratio $L/r_0 = 1/r$	Natural frequency ω_i (rad/s)	F-F			C-F			P-P			C-C		
		Present theory	Coupled Bernoulli-Euler theory [17]	% error	Present theory	Coupled Bernoulli-Euler theory [17]	% error	Present theory	Coupled Bernoulli-Euler theory [17]	% error	Present theory	Coupled Bernoulli-Euler theory [17]	% error
25	ω_1	8882.7	9075.4	2.17	1444.9	1457.9	0.90	4748.9	4875.3	2.66	8470.7	9241.6	9.10
	ω_2	22,666	24,332	7.35	8507.1	9012.0	5.94	14,752	15,678	6.28	21,171	25,058	18.4
	ω_3	40,502	41,188	1.69	20,594	20,594	0.00	31,316	35,642	13.8	37,444	41,188	10.0
	ω_4	41,188	46,099	11.9	21,912	24,701	12.7	37,185	38,386	3.23	41,188	47,922	16.4
	ω_5	60,601	73,239	20.9	38,906	46,989	20.8	51,703	62,789	21.4	55,846	76,710	37.4
50	ω_1	2296.9	2310.3	0.58	364.28	365.11	0.23	1216.5	1224.8	0.68	2267.0	2321.1	2.39
	ω_2	6190.1	6322.0	2.13	2245.1	2280.2	1.56	3984.1	4057.2	1.84	6061.2	6371.2	5.11
	ω_3	11,762	12,277	4.38	6128.0	6349.1	3.61	8939.8	9318.0	4.23	11,443	12,409	8.44
	ω_4	18,711	20,061	7.22	10,297	10,297	0.00	14,540	15,323	5.39	18,110	20,332	12.3
	ω_5	20,594	20,594	0.00	11,599	12,342	6.41	20,034	20,535	2.50	20,594	20,594	0.00
75	ω_1	1027.6	1030.3	0.26	162.16	162.32	0.10	543.18	544.85	0.31	1021.5	1032.5	1.08
	ω_2	2803.4	2830.8	0.98	1008.6	1015.7	0.70	1799.2	1814.3	0.84	2776.1	2840.7	2.33
	ω_3	5414.5	5525.8	2.06	2790.9	2836.9	1.65	4095.7	4176.1	1.96	5343.2	5552.6	3.92
	ω_4	8780.8	9086.0	3.48	5378.5	5539.1	2.99	6917.4	7130.5	3.08	8638.2	9142.1	5.83
	ω_5	12,822	13,487	5.19	6864.6	6864.6	0.00	10,747	11,280	4.96	12,580	13,588	8.01
100	ω_1	579.39	580.26	0.15	91.265	91.317	0.06	306.05	306.57	0.17	577.45	580.94	0.60
	ω_2	1587.7	1596.5	0.55	569.53	571.78	0.40	1017.8	1022.7	0.48	1578.8	1599.7	1.32
	ω_3	3085.9	3122.3	1.18	1583.9	1598.8	0.94	2329.8	2355.9	1.12	3062.2	3130.8	2.24
	ω_4	5044.0	5145.7	2.02	3073.9	3126.5	1.71	3981.4	4054.2	1.83	4995.6	5163.7	3.37
	ω_5	7432.6	7659.0	3.05	5019.6	5148.5	2.57	6218.5	6399.4	2.91	7347.9	7691.7	4.68

displacement present. The fifth mode is bending dominated, but with substantial axial deformation in the central part of the beam. The behaviour of the mode shapes for the C-C is similar to that of the F-F case in the sense, the first and fourth modes are respectively bending and axial whereas some amount of coupling between bending and axial deformation is present in the second, third and fifth mode. It is interesting to note that for the F-F, C-F and C-C boundary conditions, pure axial mode can occur (see Eqs. (30)–(32) and Eq. (35)) whereas for the P-P case this cannot happen because the pin support at the shear centre will couple the axial displacement with the bending rotation (see Eq. (30)). This observation can be further verified by the force-displacement relationship given by Eq. (50) and considering the zero and non-zero elements of the dynamic stiffness matrix and then applying appropriate boundary conditions. Another interesting observation that can be made from the results shown in Fig. 6 is that unlike the classical beam theory which gives exactly the same natural frequencies for the F-F and C-C cases (when the rigid-body modes for the F-F case are disregarded), the coupled axial-bending dynamic stiffness theory developed in this paper reveals somehow a different picture in that it gives different natural frequencies for the F-F and C-C cases. Given the complexity of the problem, this is expected. Similar observation was made for the bending-torsion coupled beams [1–4]. The results shown in Fig. 6 indicate that for the first five modes, the differences in the natural frequencies for the F-F and C-C cases are 4.67%, 6.57%, 7.53%, 0.0% and 7.85%, respectively.

In order to demonstrate the degree of inaccuracy that can creep into the result when neglecting the effects of shear deformation and rotatory inertia, Fig. 7 shows, for different values of the slenderness ratio, the percentage error (ε %) that will incur in the first three natural frequencies ($i = 1, 2$ and 3) of the beam for clamped-clamped (C-C) boundary condition when using coupled axial-bending Bernoulli-Euler theory as opposed to the current axial-bending coupled Timoshenko theory. This C-C boundary condition was chosen for illustrative purposes because the effects of shear deformation and rotatory inertia are much more pronounced for this case than for other boundary conditions which was also observed in earlier investigation of natural frequencies using classical (uncoupled) Timoshenko beam theory [26]. Clearly, with increasing values of the slenderness ratio, the error diminishes, as expected.

One of the striking features of the Timoshenko beam theory is that it

assumes the shear rigidity (kAG) of the beam to have a finite value which is approximately of the same order of magnitude of the axial or extensional rigidity (EA) which is in sharp contrast to the Bernoulli-Euler theory which assumes implicitly that the shear rigidity of the beam to be infinite. It is well recognised that Timoshenko introduced a fictitious shear correction factor (also known as the shape factor) k to account for the zero shear-stress condition at the free surface of the beam. The value of k essentially provides an indicative effectiveness of the cross-section in carrying the shear stress. The value of k can be realistically taken within the range $0.4 < k < 0.9$ depending on the type of cross-section. In all the above illustrative examples, the value of k was taken to be 2/3. To demonstrate the effect of k on results, Fig. 8 shows for a range of k values, the percentage error (ε %) in the first two natural frequencies of the above example for C-C boundary condition with the slenderness ratio $L/r_0 = 25$ when the coupled axial-bending Bernoulli-Euler theory is used as opposed to coupled axial-bending Timoshenko theory. The first two natural frequencies were chosen because the modes corresponding to these natural frequencies are dominated by bending deformation for which the shear correction factor is expected to have a major effect. As expected, Fig. 8 shows that with increasing values of k, the error diminishes. For a typical value of $k = 0.7$, error incurred in the two natural frequencies are 8.7% and 17.5%, respectively.

The next set of results was obtained for a portal frame shown in Fig. 9. The properties for each of the three beams which make the portal frame are taken to be the same as those of the single beam used above, but the length (L) of each beam is set to 0.5 m. Table 3 shows the first five natural frequencies of the portal frame computed using the current DSM based on coupled axial bending Timoshenko theory together with the ones computed using the earlier DSM theory based on coupled axial bending Bernoulli-Euler theory [17]. Predictably, the earlier theory [17] which neglects the effects of shear deformation and rotatory inertia overestimates the natural frequencies. The errors are expected to be larger for bending dominated higher order modes. For frameworks, however, the error may not increase in any predictable manner, i.e. with ascending order or descending order of the natural frequencies, given the complexity of the problem, associated with the coupling effect arising from the axial and bending deformation. For instance, the errors incurred in the fourth and fifth natural frequencies, as a result of using coupled axial-bending Bernoulli-Euler dynamic stiffness theory as opposed to the corresponding Timoshenko theory of the current paper
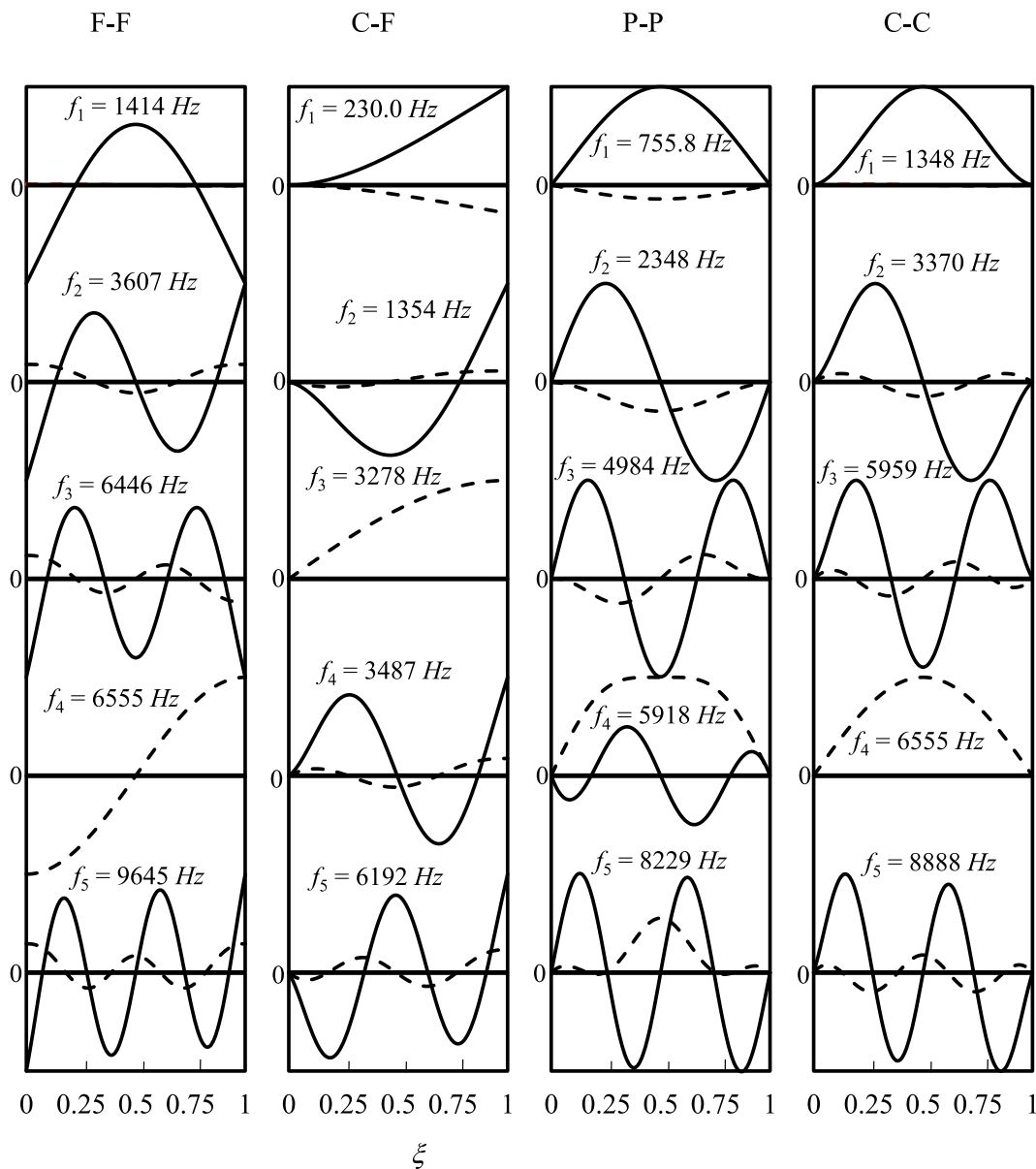
Fig. 6. Natural frequencies and mode shapes of a coupled axial-bending Timoshenko beam with slenderness ratio 25 for F-F, C-F, P-P and C-C boundary conditions. ——— W; ········· V.
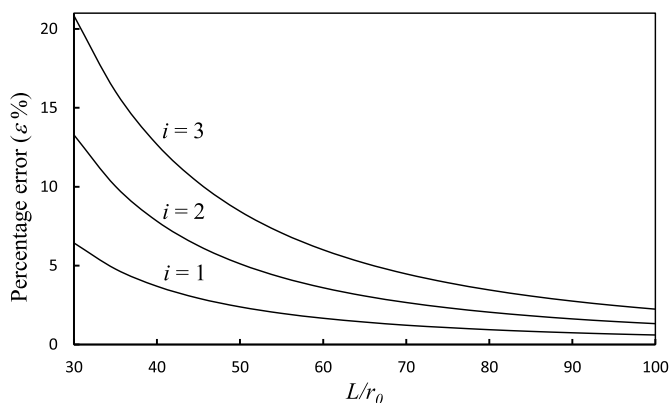

Fig. 7. The effect of the slenderness ratio on the percentage error in the first three natural frequencies for Clamped-Clamped (C-C) boundary condition of a coupled axial-bending beam when using Bernoulli-Euler theory as opposed to Timoshenko theory.

are 5.35% and 4.74% respectively. The mode shapes of the portal frame computed using the present theory are shown in Fig. 10.

The final set of results was obtained for a continuous beam shown in Fig. 11 which is a much bigger structure than the ones chosen in previous examples. The cross-section of the continuous beam is uniform and is an inverted T section (Fig. 4), but with the dimension $b = 15$ cm, $t = 1$ cm. The materials used is that of steel with Young's modulus $E = 200$ GPa, shear modulus $G = 76.92$ GPa and density, $\rho = 7850$ kg/m^3. The shear correction factor k is set to 2/3. The properties of the cross-section as required for the analysis are calculated as follows.

(i) Axial stiffness (EA) $= 5.8 \times 10^8$ N, (ii) Bending stiffness (EI_e) $= 2.034833 \times 10^6$ Nm^2, (iii) Shear stiffness (kAG) $= 1.4872 \times 10^8$ N, (iv) Mass per unit length (ρA) $= 22.765$ kg/m, (v) Rotatory inertia per unit length (ρI_e) $= 0.079867$ kgm and the (vi) Distance between the shear centre and centroid (z_α) $= 0.036207$ m.

The first eight natural frequencies of the continuous beam (see Fig. 11) are computed using the present theory and shown in Table 4
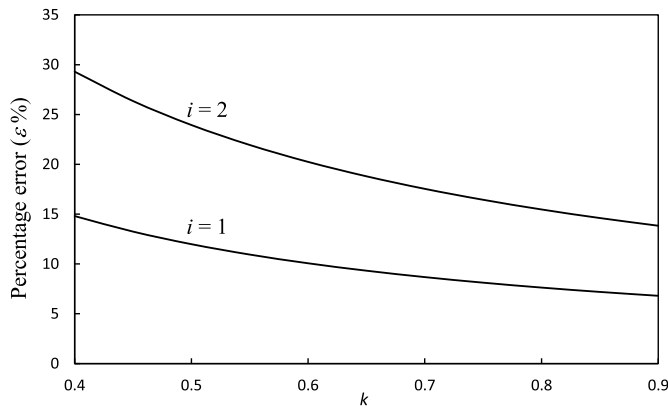
Fig. 8. The effect of the shear correction factor (shape factor) k on the percentage error (ε%) for the first two natural frequencies of a coupled axial-bending beam with slenderness ratio $L/r_0 = 25$ and for Clamped-Clamped (C-C) boundary condition when using Bernoulli-Euler theory as opposed to the Timoshenko theory.
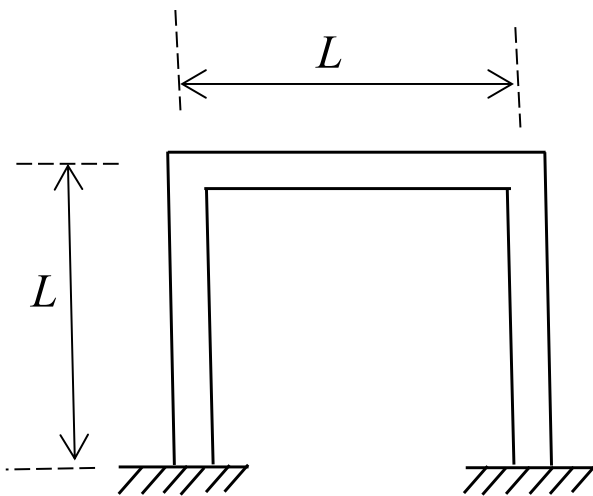

Fig. 9. A portal frame comprising coupled axial-bending Timoshenko beams.

Table 3
Natural frequencies of a portal frame using coupled axial-bending Timoshenko and Bernoulli-Euler theories.

Natural frequency number (i)	Natural frequency ω_i (rad/s)		% Difference
	Present Theory	Coupled axial-bending Bernoulli-Euler theory [17]	
1	792.69	803.19	1.32
2	2906.4	2966.2	2.06
3	4848.7	5036.4	3.87
4	5160.4	5436.2	5.35
5	9432.2	9879.4	4.74

together with the results computed using the earlier coupled axial-bending Bernoulli-Euler theory [17] which neglected the effects of shear deformation and rotatory inertia. The modes dominated by axial deformation is denoted by A whereas the bending dominated modes are denoted by B. The modes with substantial coupling between the axial and bending deformations are indicated by the letter C. As it can be seen, there are significant differences in the natural frequencies, particularly for the higher order bending dominated modes and also for coupled modes when the results from the current coupled axial-bending Timoshenko theory are compared with the earlier coupled axial-bending
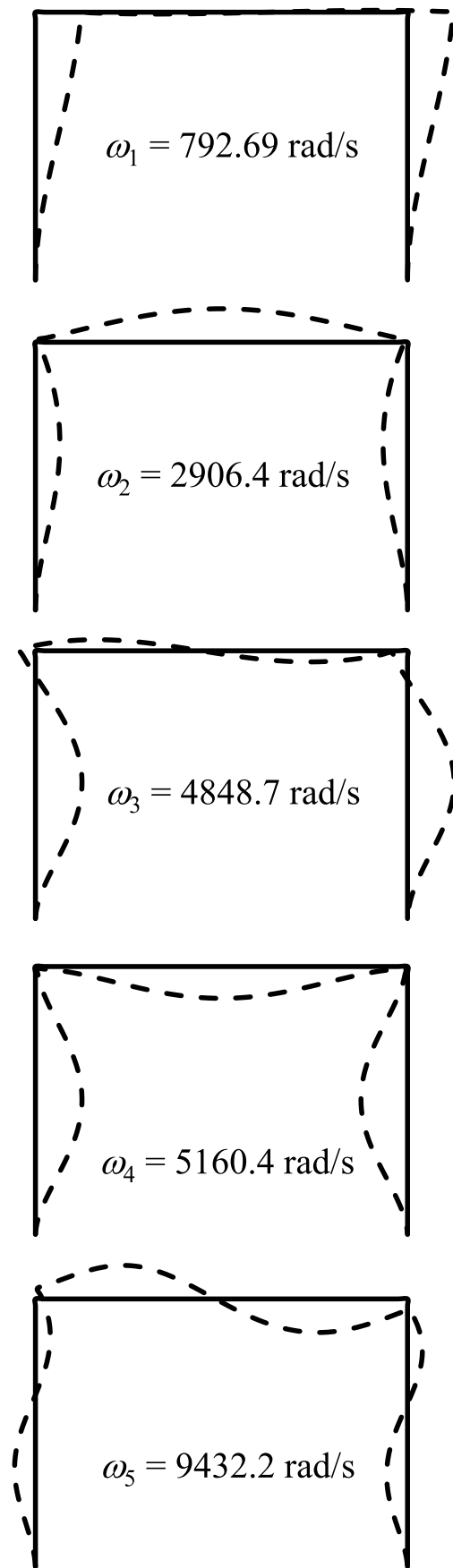

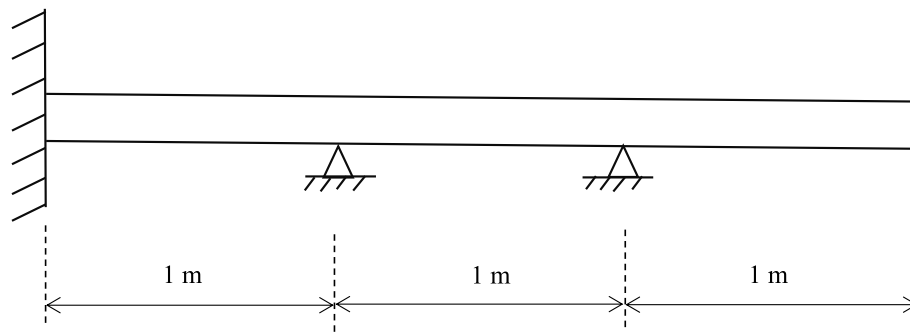**Fig. 10.** Mode shapes of a portal frame using coupled axial-bending Timoshenko theory.

Fig. 11. A continuous beam with the inverted T cross-section of Fig. 4.

Table 4
Natural frequencies of a continuous beam using coupled axial-bending Timoshenko and Bernoulli-Euler theories.

Natural frequency number (i)	Natural frequency ω_i (rad/s)		% Difference
	Present Theory	Coupled Bernoulli-Euler theory [17]	
1	580.95 (B)	593.99 (B)	2.25
2	2955.2 (B)	3155.7 (B)	6.79
3	3824.2 (B)	4230.3 (B)	10.6
4	4434.8 (B)	5165.3 (B)	16.5
5	7465.0 (A)	7614.1 (A)	2.00
6	8708.7 (C)	10,009 (B)	14.9
7	9962.5 (B)	12,299 (B)	23.5
8	10,623 (B)	13,782 (B)	29.7

Bernoulli-Euler theory [17]. For axial dominated natural frequency such as the fifth natural frequency shown in Table 4, the effects of shear deformation and rotatory inertia are not so pronounced, as expected.

4. Conclusions

Using the Timoshenko beam theory, the dynamic stiffness matrix of a coupled axial-bending beam is developed. The governing differential equations are derived using Hamilton's principle and they are solved in closed explicit analytical form in terms of trigonometric and hyperbolic functions. Unlike previous investigations which showed that six arbitrary constants are needed to describe axial displacement, bending displacement and bending rotation, the current investigation revealed that only four arbitrary constants are needed to describe the bending displacement and bending rotation whereas six arbitrary constants are needed to describe the axial displacement. The dynamic stiffness matrix of the axial-bending coupled Timoshenko beam is formulated by relating the amplitudes of the forces to those of the corresponding displacements of the harmonically vibrating beam. The frequencies and mode shapes are computed by applying the Wittrick-Williams algorithm as solution technique. The theory is validated by an ingeniously devised numerical scheme in which the coupled axial-bending Timoshenko beam is approximated by a well-established computer program BUNVIS-RG that uses uncoupled classical beam theories. Carefully selected results are given to demonstrate the importance of shear deformation and rotatory inertia in the free vibration of axial-bending coupled beams with various boundary conditions. Representative mode shapes are presented showing coupling between axial and bending deformations. The theory is further applied to a portal frame and to a continuous beam for which natural frequencies computed from simpler Bernoulli-Euler axial-bending coupled theory are compared and contrasted. It is in the context of the free vibration analysis of axial-bending coupled beam, particularly in the medium to high frequency range, the proposed theory is expected to be most effective. The results presented can be used as an aid to validate finite element and other approximate methods.

CRediT author statement

J R Banerjee: Developed the broad outline of the theory, interpreted results and supervised the overall development of the paper. A Ananthapuvirajah: Obtained numerical results, plotted graphs and looked after the presentational aspects of the paper. Took active part in the design and layout of the paper. X. Liu: Took active part in the theoretical development of the paper and provided further insights into the investigation. Was responsible for the enrichment of the ideas put forward in the paper. C. Sun: Assisted in the validation and verification of the theory and numerical results.

Declaration of competing interest

The authors declare that they have no known competing financial interests or personal relationships that could have appeared to influence the work reported in this paper.

Acknowledgements

References

[1] J.R. Banerjee, Coupled bending-torsional dynamic stiffness matrix for beam elements, Int. J. Numer. Methods Eng. 28 (6) (1989) 1283–1298, https://doi.org/10.1002/nme.1620280605.

[2] R. Butler, J.R. Banerjee, Optimum design of bending-torsion coupled beams with frequency or aeroelastic constraints, Comput. Struct. 60 (5) (1996) 715–724, https://doi.org/10.1016/0045-7949(95)00451-3.

[3] S.M. Hashemi, M.J. Richard, Free vibrational analysis of axially loaded bending-torsion coupled beams: a dynamic finite element, Comput. Struct. 77 (6) (2000) 711–724, https://doi.org/10.1016/S0045-7949(00)00012-2.

[4] R.E.D. Bishop, S.M. Cannon, S. Miao, On coupled bending and torsional vibration of uniform beams, J. Sound Vib. 131 (3) (1989) 457–464, https://doi.org/10.1016/0022-460X(89)91005-5.

[5] J.R. Banerjee, Modal analysis of sailplane and transport aircraft wings using the dynamic stiffness method, J. Phys. Conf. Ser. 721 (1) (2016), 012005, https://doi.org/10.1088/1742-6596/721/1/012005.

[6] J.R. Banerjee, X. Liu, H.I. Kassem, Aeroelastic stability analysis of high aspect ratio aircraft wings, J. Appl. Nonlinear Dyn. 3 (4) (2014) 413–422, https://doi.org/10.5890/JAND.2011.12.001.

[7] M. Lillico, R. Butler, S. Guo, J.R. Banerjee, Aeroelastic optimisation of composite wings using the dynamic stiffness method, Aeronaut. J. 101 (1997) 77–86, https://doi.org/10.1017/S0001924000066744.

[8] A.S. Yigit, A.P. Christoforou, Coupled axial and transverse vibrations of oilwell drillstrings, J. Sound Vib. 195 (4) (1996) 617–627, https://doi.org/10.1006/jsvi.1996.0450.

[9] S.M. Han, H. Benaroya, Coupled transverse and axial vibration of a compliant tower: comparison of linear and nonlinear models, in: 41st. Struct. Struct. Dyn. Mater. Conf. Exhib., 2000, p. 1347, https://doi.org/10.2514/6.2000-1347.

[10] M.A. Trindade, C. Wolter, R. Sampaio, Karhunen-Loève decomposition of coupled axial/bending vibrations of beams subject to impacts, J. Sound Vib. 279 (3–5) (2005) 1015–1036, https://doi.org/10.1016/j.jsv.2003.11.057.

[11] R. Sampaio, M.T. Piovan, G. Venero Lozano, Coupled axial/torsional vibrations of drill-strings by means of non-linear model, Mech. Res. Commun. 34 (5–6) (2007) 497–502, https://doi.org/10.1016/j.mechrescom.2007.03.005.

[12] J.H. Ginsberg, Coupling of axial and transverse displacement fields in a straight beam due to boundary conditions, J. Acoust. Soc. Am. 126 (3) (2009) 1120–1124, https://doi.org/10.1121/1.3183368.

[13] S. Lenci, G. Rega, Axial-transversal coupling in the free nonlinear vibrations of Timoshenko beams with arbitrary slenderness and axial boundary conditions, Proc. Roy. Soc. A. Math. Phys. Eng. Sci. 472 (2190) (2016), 20160057, https://doi.org/10.1098/rspa.2016.0057.

[14] Z. Lei, J. Su, H. Hua, Longitudinal and transverse coupling dynamic properties of a Timoshenko beam with mass eccentricity, Int. J. Struct. Stabil. Dynam. 17 (7) (2017), 1750077, https://doi.org/10.1142/S0219455417500778.

[15] Z. Ni, H. Hua, Axial-bending coupled vibration analysis of an axially-loaded stepped multi-layered beam with arbitrary boundary conditions, Int. J. Mech. Sci. 138–139 (2018) 187–198, https://doi.org/10.1016/j.ijmecsci.2018.02.006.

[16] A. Tomović, S. Šalinić, A. Obradović, A. Grbović, M. Milovančević, Closed-form solution for the free axial-bending vibration problem of structures composed of rigid bodies and elastic beam segments, Appl. Math. Model. 77 (2020) 1148–1167, https://doi.org/10.1016/j.apm.2019.09.008.

[17] J.R. Banerjee, A. Ananthapuvirajah, Coupled axial-bending dynamic stiffness matrix for beam elements, Comput. Struct. 215 (2019) 1–9, https://doi.org/10.1016/j.compstruc.2019.01.007.

[18] J.R. Banerjee, A. Ananthapuvirajah, An exact dynamic stiffness matrix for a beam incorporating Rayleigh–Love and Timoshenko theories, Int. J. Mech. Sci. 150 (2019) 337–347, https://doi.org/10.1016/j.ijmecsci.2018.10.012.

[19] F.W. Williams, W.H. Wittrick, Exact buckling and frequency calculations surveyed, J. Struct. Eng. 109 (1) (1983) 169–187, https://doi.org/10.1061/(ASCE)0733-9445(1983)109:1(169).

[20] W.H. Wittrick, F.W. Williams, A general algorithm for computing natural frequencies of elastic structures, Q. J. Mech. Appl. Math. 24 (3) (1971) 263–284, https://doi.org/10.1093/qjmam/24.3.263.

[21] J.R. Banerjee, A.J. Sobey, H. Su, J.P. Fitch, Use of computer algebra in Hamiltonian calculations, Adv. Eng. Software 39 (6) (2008) 521–525, https://doi.org/10.1016/j.advengsoft.2007.03.013.

[22] J.R. Banerjee, F.W. Williams, Free vibration of composite beams- an exact method using symbolic computation, J. Aircraft 32 (3) (1995) 636–642, https://doi.org/10.2514/3.46767.

[23] J. Fitch, Solving algebraic problems with REDUCE, J. Symbolic Comput. 1 (2) (1985) 211–227, https://doi.org/10.1016/S0747-7171(85)80015-8.

[24] M.S. Anderson, F.W. Williams, J.R. Banerjee, B.J. Durling, C.L. Herstorm, D. Kennedy, D.B. Warnaar, NASA Technical Memorandum 87669, in: User Manual for BUNVIS-RG: an Exact Buckling and Vibration Program for Lattice Structures, with Repetitive Geometry and Substructuring Options, 1986.

[25] M.S. Anderson, F.W. Williams, BUNVIS-RG: exact frame buckling and vibration program, with repetitive geometry and substructuring, J. Spacecraft Rockets 24 (4) (1987) 353–361, https://doi.org/10.2514/3.25924.

[26] J.B. Carr, The effect of shear flexibility and rotatory inertia on the natural frequencies of uniform beams, Aeronaut. Q. 21 (1) (1970) 79–90, https://doi.org/10.1017/S0001925900005242.